A Model-Chain to Generate Q/V Band Attenuation Time Series from Short-Term Numerical Weather Predictions at Continental Scale

M. Biscarini, *Senior Member, IEEE*, R. Nebuloni, L. Dossi, S. Di Fabio, P. Scaccia, T. Cherubini, C. Riva, *Senior Member, IEEE*, and L. Luini, *Senior Member, IEEE*

***Abstract*— To minimize the impact of propagation impairments occurring at Ka-band and beyond, satellite communication systems operating at such high frequencies require the implementation of adaptive fade mitigation techniques (FMTs). As beacon measurements are rarely available (especially with the spatial distribution and the time resolution required by FMTs), time series generators represent a key tool for the design stage of such systems. This paper proposes a novel three-module model chain to generate time series of rain attenuation. The first module is a Numerical Weather Prediction (NWP) model that forecasts meteorological parameters across a continental grid with 9 km × 9 km and 15-min resolution in space and time, respectively. The NWP model outputs feed a radiopropagation model, which produces time series of the attenuation components (gas, clouds and rain). Finally, the rain attenuation is generated ex-novo at a 1-sec sampling rate, by taking advantage of the multisite time-series synthesizer (MTS). Each step of the process is validated against measurements covering a 28-day period.**

***Index Terms*—NWP, Q/V-band, rain attenuation, satellite communication, time series generators.**

I. Introduction

As the frequency bands typically used by Satellite Communication (SatCom) systems for fixed services, i.e. C- and Ku-bands, are heavily congested [1], operators are moving or already moved to higher bands, such as Ka and Q/V, which allow larger signal bandwidths and more compact antennas. However, at Ka-band and beyond, the stochastic nature of the atmospheric propagation channel produces increasingly heavy signal impairments with high dynamic range [2]. Hence, SatCom systems operating at these frequencies need to implement adaptive Fade Mitigation Techniques (FMTs) to meet the quality-of-service targets, e.g., service availability and data throughput, by optimizing the system resources in real time, rather than relying on simple techniques based on fixed power margins [3]. As a practical implementation of such systems, we can mention the recently launched Eutelsat KONNECT and Hughes JUPITER 3 that are examples of very high-throughput satellites (VHTS) with a Ka-band capacity of 500 Gbps and Q/V-band gateways [4], [5].

The design, test and validation of adaptive FMTs requires an accurate characterization of the atmospheric propagation channel. Specifically, the concentration of atmospheric constituents, like gas, and of atmospheric particles, like cloud droplets and raindrops, must be estimated [6][7], as well as their spatial and temporal distribution [8]. Moreover, propagation impairments depend on signal frequency and polarization and on the geometry of the ground-to-satellite link.

Although the evaluation of adaptive FMTs has been partially carried out based on measurements [9], there are few available experimental data, especially in the Q/V band, and rarely collected over a lapse of time long enough to capture the seasonal and yearly variability of the processes. Some quite satisfactory, in terms of time duration of collected measurements, databases across Europe are provided by the Olympus [10] and the Italsat [11] programs: the first two main European initiatives, dating back to the 1980s, to verify the viability of 20-50 GHz atmospheric channel through accurate measurements of propagation conditions [12]. The more recent Alphasat campaign at Ka and Q band has produced (and is still producing) more temporally extensive data [13]. Such databases are limited to single geographical sites and up to Q band. Hence, there are no measurements on large areas, required for the implementations of some FMTs such as the smart gateway diversity, with climatological value, especially up to V band. Hence, resorting to propagation models and simulations is a common practice. In particular, time series generators of propagation-related quantities, such as path attenuation, are key tools. Moreover, if FMTs involve the simultaneous assessment of propagation conditions across

M. Biscarini is with the Department of Information Engineering, Electronics and Telecommunications (DIET), Sapienza University of Rome, 00184 Rome, Italy, (e-mail: marianna.biscarini@uniroma1.it).

R. Nebuloni and L. Dossi are with the Consiglio Nazionale delle Ricerche, (CNR-IEIIT), Milano, Italy (e-mail: roberto.nebuloni@ieiit.cnr.it; laura.dossi@ieiit.cnr.it).

S. Di Fabio is with the Center of Excellence Telesensing of Environment and Model Prediction of Severe events (CETEMPs), L'Aquila, Italy and with HIMET, L'Aquila, Italy (saverio.difabio@aquila.infn.it).

P. Scaccia is with AdaptiveMeteo, Rome, Italy (paolo.scaccia@adaptivemeteo.com).

T. Cherubini is with University of Hawaii, Dept. of Meteorology, Honolulu, Hawaii, USA (tiziana@hawaii.edu).

L. Luini and C. Riva are with the Department of Electronics, Information and Bioengineering (DEIB), Politecnico di Milano, Milan, Italy (e-mail: lorenzo.luini@polimi.it; carlo.riva@polimi.it).

several links, as in the case of techniques based on spatial diversity (e.g. smart gateway diversity [14]), attenuation time series should be obtained in multiple sites and should reproduce the spatial correlation of the processes as well. In addition, especially when smart gateway diversity must be implemented, a time-resolution of 1 second is required in order to properly design and plan the switch from the gateway in outage, typically due to rain affecting the link, to the backup gateway [9].

Attenuation time series can be obtained by resorting to machine learning techniques, as in [15], or through stochastic generators. ITU-R Rec. P.1853-2 [16] provides practical implementation rules for generating time series of the components of tropospheric attenuation for Earth-space links. ITU-R algorithms are based on analytical models for the shape of the CCDF of each component, as well as for their temporal and spatial correlation, which hold on a climatological basis. Hence, they are more suitable to reproduce the long-term features of the channel. Several time series generators are built upon the mathematical framework proposed in the early work of Maseng and Bakken [17], which models rain attenuation as a first order Markov random process with a lognormal CCDF (complementary cumulative distribution function). The process is characterized by three-parameters: μ and σ of the lognormal CCDF (i.e., mean and standard deviation, respectively, of the variable's natural logarithm) and β, which defines the temporal autocorrelation function of the process. The enhanced version of the Maseng and Bakken model in [18] modifies the lognormal distribution to account for the local probability of rain. The authors in [18] also propose methods for generating synthetic events with user-defined properties and for carrying out a stochastic interpolation of existing time series. The Multisite Time series Synthesizer (MTS) in [19] generates N sequences of rain attenuation bounded by dry periods in as many sites. Rain attenuation events are randomly extracted from a database of measurements. The process is subject to the following conditions: a) the time series must fit N user-defined CCDFs; b) the N time series must be spatially correlated according to the reciprocal distance among the sites.

An alternative to random process generators is to produce the time series from the outcomes of Numerical Weather Prediction (NWP) models. NWPs implement a mathematical description of the thermodynamic state of the atmosphere and their outputs provide the inputs required by several physically-based propagation models [20]. Another advantage of NWPs is that they can generate the temporal evolution of the 3D layered forecasts of the atmospheric variables over large areas, hence they can be used for both GEO (Geostationary Earth Orbit) and non-GEO systems. However, the exploitation of NWP data for SatCom applications has been only partially investigated so far: these products can seldom achieve fine spatial and temporal resolutions, due to the extremely high computation burden, while providing a good accuracy. Indeed, predicting heavy and localized, both in space and in time, precipitation events, which may result in link outage, hence in service loss, is still a challenge for NWPs. Another limitation is the growing computing time and storage volume when the forecast is generated over large grids. Although NWP products are not mature enough for their operational use in SatCom control chains, nonetheless they can be beneficial for the system design stage: the NWP data can be used for the design of the adaptive FMTs (especially smart-gateway diversity), imagining that each grid point or a subset of grid points where NWP are available correspond to positions of the gateways or user terminals.

Indeed, in [21] and [22], NWP outputs combined with propagation models were used to generate time series of rain and cloud attenuation with a resolution up of 2 km in space and 5-min in time, respectively. A gateway switching control algorithm based on weather forecasts is proposed in [23], suitable for applications in which switching rates are low, e.g., from 1 hour to 1 day. Recently, high-resolution time series of the rain attenuation have been produced through a model chain based on a cascade of a NWP model, a rainfall cell generator and an optical flow algorithm [24]. The tool provides a time resolution of 1-min over a limited geographical area in Belgium of about 160 km ×160 km.

This work presents a novel model chain to generate time series of path attenuation. The novelty relies in the exploitation of NWPs products to drive the generation of time-series with 1-sec temporal resolution. The model, developed in the framework of the ESA project RadioSatMet [25], aims at providing high-resolution time series in multiple sites for the assessment of adaptive FMTs over a continental scale, which is the ultimate goal of the project. The RadioSatMet model chain includes three major functional blocks. The NWP model is cascaded with a parametric radiopropagation model (PRM) and the aforementioned MTS to increase the resolution of the resulting time series to 1 second. First results concerning the implementation of the first two blocks (NWP+PRM) were presented in [26]. An important point is that, differently from its original conception [19], in this contribution the MTS tool is challenged to simulate relatively short time series of 28 days.

Compared to other approaches already existing in literature and previously discussed, the advantages of the proposed RadioSatMet model are: i) capability of producing high resolution time-series of attenuation down to 1-sec thanks to the MTS module; ii) possibility of designing mitigation techniques requiring fast adaptive times such as smart-gateway-diversity with switching latency and switching rates of few seconds; iii) production of attenuation maps on a continental scale potentially exploitable for SatCom system applications.

The RadioSatMet blocks are detailed in Section II, while in Section III the model chain is validated based on experimental data. Finally, the conclusions are drawn in Section 0.

II. Model-Chain for Time Series Generation

Fig. 1 describes the proposed model-chain for the time series generation. The final goal is to provide time series of radiopropagation quantities (i.e., atmospheric attenuation and brightness temperature) on a regular continental grid (i.e. the SatCom coverage area).

The first step of the process is a single-domain NWP model described in section II.A. The process generates daily forecasts of atmospheric quantities at a medium-high spatial resolution of

9 km × 9 km every 15-min over the SatCom coverage area. Furthermore, to better characterize the two Italian sites of Tito Scalo (TS) and Spino d'Adda (SdA), where Alphasat measurements are available for validation [28], forecasts at high time resolution of 30 seconds are produced only on the two single pixels of Tito Scalo and Spino d'Adda. NWPs are obtained as the output of the Advanced Research Weather Research Forecast model, WRF-ARW, hereafter referred to simply as WRF [27], which is initialized with global-scale data. Secondly, atmospheric quantities are converted into radiopropagation variables through the PRM (section II.B). The outputs are the time series of atmospheric attenuation and brightness temperature with 15-min time resolution. Thirdly, the PRM-derived time series of the rain attenuation component are elaborated to synthesize new time series at a much higher time rate of 1 second by means of the MTS tool (section II.C). This last step is mandatory since the time series are used for the design and test of FMTs able to update the SatCom system configuration according to the dynamics of the atmospheric channel: indeed, at Ku- and higher bands, precipitation drives the rate and intensity of signal variations.

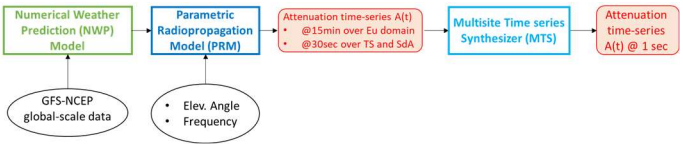

Fig. 1 Proposed model-chain for time series generation. Rectangular blocks denote the operational modules: Numerical Weather Prediction (NWP) model, parameterized radiopropagation model (PRM), and multi-site time series synthesizer (MTS). Elliptical blocks are the external input data and rounded red smoothed rectangular blocks are the outputs produced by the model-chain.

A. Numerical Weather Prediction (NWP) Model

NWPs are produced resorting to WRF model, developed and supported as a community model by the National Center for Atmospheric Research (NCAR) [27]. The WRF modeling system supports atmospheric simulations across scales from high-resolution (large-eddy) to global. WRF integrates the compressible, nonhydrostatic Euler equations and includes several options for microphysics, cumulus parameterization, planetary boundary layer, land-surface model, and radiation.

For this work, the WRF model uses the Global Forecast System (GFS) model analyses and forecast provided by the National Centers for Environmental Prediction (NCEP), as initial and boundary conditions.

The chosen WRF model configuration encompasses a mid-latitude European domain, referred to as d01, with horizontal grid spacing of 9 km and a size of approximately 5000 km × 3000 km (Fig. 2). WRF simulations are started at every synoptic hour (00:00, 06:00, 12:00 and 18:00 UTC) for four full weeks in the timeframe from 21 April 2020 to 31 May 2020 and each model forecast is 24 hours long. The 3-dimensional WRF model output for the entire European domain is saved with a 15-minute frequency and used as input to the PRM model. In addition, as previously stated, time-series of the main prognostic variables from the nearest model grid point to the two stations of Tito Scalo and Spino d'Adda are recorded at every integration time-step of the model that, in our case, is every 30 seconds. This latter dataset includes the following meteorological parameters required by the PRM: pressure, temperature, humidity, hydro-meteors distribution (e.g., rain, ice, graupel etc.), wind intensity and direction. The main WRF configuration and settings are summarized in Table I.

The "best day" forecast is compiled by selecting the best 6 hours from each of the four daily runs. Notably, the initial 6 hours of each run are affected by the model spin-up, i.e., the time required by the model to properly propagate the boundary and initial conditions in the whole domain. Consequently, within the 24 hours forecast of a single run, the "best 6 hours" correspond to the ones closest to the initialization time but just after the spin-up. With four runs every 6 hours, the 'best day', i.e., the best 24 hours, is identified by considering the four "best 6-hour slots" from each run. This operational procedure is common, as weather forecasts often prioritize hours immediately following the model spin-up and closest to the initialization time.

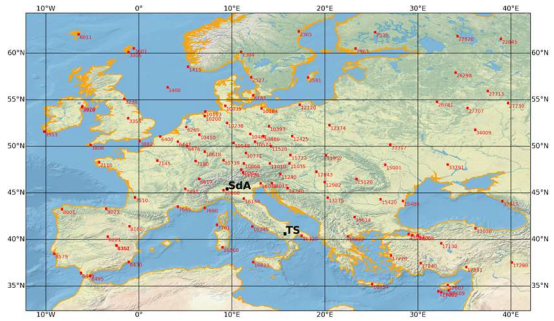

Fig. 2 Continental (European) domain used for the model-chain simulations including Tito Scalo and Spino d'Adda sites (TS and SdA, respectively). The radiosondes used for the WRF model validation are highlighted as well (red dots).

TABLE I
NWP CONFIGURATION AND SETUP (WRF MODEL AT 9 KM SPACE RESOLUTION)

Domain	*d01*	*Single grid-point*
Coverage	Europe (3000 km×5000 km)	Single point: Tito Scalo or Spino d'Adda
Time resolution	15 min	30 sec
Grid size	350×400	1x1
Initialization	GFS-NCEP	Extraction from d01 run

B. Parametrized Radiopropagation Model (PRM)

The PRM model receives as input the meteorological forecasts generated by the NWP model at each d01 grid-point or the higher temporal resolution time-series from the nearest model grid point to the two Alphasat stations and converts them into radiopropagation parameters with the same resolution in space and in time as the one used by NWP model. The PRM outputs are:

- path integrated total attenuation and individual components (i.e. rain, cloud, water vapor and oxygen attenuation);
- brightness temperature.

The above quantities are calculated along the zenithal path and then rescaled at the considered elevation angle through the cosecant law at each grid point assuming a GEO SatCom system with a satellite located a 25°E longitude (i.e., the longitude of the Alphasat satellite). Note that, especially for geostationary links operating with midlatitude ground stations at elevation angles ranging around 30° - 40° (as in our case, where elevation angles in Tito and Spino are 42.1° and 35.5°, respectively), the error

committed by adopting the cosecant low is expected to be negligible if compared to other available models [28], [29]. The frequencies selected for the simulations are: 19.7, 30.0, 38.0, 39.4, 48.0, and 50.9 GHz.

The absorption due to water vapor and oxygen is parametrically related to pressure, temperature and water vapor mixing ratio. The latter are provided by the NWP model and then properly combined in order to obtain the specific attenuation due to gas (k_{gas}, in dB/km) as the sum of oxygen (k_{o_2}) and water vapor (k_{H_2o}) contributions, according to the standard models included in [31]: $k_{gas} = k_{o_2} + k_{H_2o}$ (dB/km).

The specific attenuation due to rain and clouds is calculated from the particle density ρ, through the power-law relationship

$$k_i = a_i \rho_i^{b_i} \quad \text{(dB/km)} \tag{1}$$

where the subscript i indicates the water particle type, i.e., *cl* for cloud and *r* for rain. The regression coefficients a_i and b_i are obtained from an available data set previously calculated for each particle by means of the T-matrix electromagnetic scattering approach. T-matrix is an open source code that allows for the computation of scattering effects from spheroidal particles at the frequency and incidence angles of interest by properly selecting a particle axial ratio and considering the particle size distribution, density, shape and orientation [32]. A very useful reference database concerning the applicability of the T-matrix model at microwave frequencies is provided in [33]. The hydrometeor density ρ_i required for calculating the specific attenuation in (1) is obtained from the particle mixing ratio Q_i (g/kg), available from NWP model outputs, using the ideal gas law

$$\rho_i = (Q_i p)/(RT) \quad \text{(g/m}^3\text{)} \tag{2}$$

where p is the atmospheric pressure (Pa), T is the absolute temperature (K) and R = 287.05 (J/(kg·K)) is the specific gas constant for dry air. The specific attenuation due to the water particles k_{wp} is

$$k_{wp} = k_r + k_{cl} \quad \text{(dB/km)} \tag{3}$$

and the total specific attenuation k_{tot} is:

$$k_{tot} = k_{gas} + k_{wp} \quad \text{(dB/km).} \tag{4}$$

Finally, the total attenuation A_t is obtained by integrating k_{tot} along the zenith from the surface (z=*0*) to the top of the troposphere, i.e., the highest vertical level simulated by WRF (z=h), and by rescaling it to the link elevation angle θ using the cosecant law:

$$A_t(\theta) = \text{cosec}(\theta) \int_0^h k_{tot}(z)dz \quad \text{(dB)} \tag{5}$$

Although this work focuses on attenuation time-series generation, it is worth mentioning that, in the most comprehensive framework of applicability of FMTs to SatCom systems, the possibility of producing time-series of brightness temperature is anyway important. For this reason, the brightness temperature T_B in (K) is also an output of our model chain and is parametrically related to the path attenuation through the well-known equation [31]

$$T_B(\theta) = T_c e^{-A_t(\theta)/4.343} + T_{mr}\left(1 - e^{-A_t(\theta)/4.343}\right) \quad \text{(K)} \tag{6}$$

where T_c = 2.73 (K) is the cosmic background radiation temperature and T_{mr} is the mean radiative temperature (K). The latter is retrieved by resorting to the Generalized Parametric Prediction (GPP) Model described in [34], which provides the mean radiative temperature in all-weather conditions as a function of the corresponding value of the atmospheric attenuation and the surface meteorological temperature.

C. Multisite Time Series Synthesizer (MTS)

At Ka-band and beyond, rain is the dominant component of the total attenuation when we consider the small percentages of time corresponding to the maximum outage tolerated by SatCom services, typically 1% at European latitudes, where mainly a temperate climate is expected. Moreover, heavy rain at these frequencies produces link outages. Finally, path loss variations due to rain are fast and in the order of a few seconds. Since adaptive FMTs are typically implemented to mitigate the effects of rain, it is important to resort to accurate models generating rain attenuation time series with a time step fine enough to implement FMTs.

In the RadioSatMet model chain, the resolution of the rain attenuation time series generated by PRM is refined to 1 second by a stochastic method based on the MTS [19]. The MTS generates time series by combining the rain events extracted from a database of more than 2500 hours of rain attenuation measurements (1 sample/s) that were collected at the three available beacon frequencies (18.7, 39.6, and 49.5 GHz) at the ground station of Spino d'Adda, Italy, during the Italsat experiment (1994–2000) [35].

The MTS inputs are a set of N ground sites (corresponding, for instance, to the locations of the N gateways within a SatCom system, where the time series must be generated), the link characteristics (satellite position, frequency and polarization), and the 15-min rain attenuation time series generated by the PRM in the grid-points corresponding to the N sites. The PRM data are processed to obtain the Complementary Cumulative Distribution Function (CCDF) of the rain attenuation over a certain observation period, which constitutes the objective CCDF. The process is sketched in Fig. 3. The time series are generated in two steps: 1) N binary time series of dry/rainy periods are created, and 2) events are extracted from the Italsat database to fill the rainy periods. To this aim, Italsat events are classified in advance according to peak attenuation (9 classes) and duration (23 classes). Each objective CCDF is fitted by a linear combination of the CCDFs of the 9 peak attenuation classes (which are normalized to 1 since, being rain-attenuation CCDFs, their highest probability level will be less than 1). The weight of each contributing CCDF multiplied by the size of the total simulated time represents the duration of all the events to be extracted from that peak attenuation class. The dry/rainy periods are generated based on the probability that it is raining along the path, calculated from the initial point of each objective CCDF. These periods are multiple of a basic 5-min slot, as this is the minimum duration of the Italsat events. Finally, the dry/rainy state binary process and the rain attenuation process are spatially correlated assuming the models in [36] and [37], to which the reader is addressed for

further details. The temporal correlation of the binary process is assumed exponential, while the temporal correlation of rain attenuation is inherently embedded in the Italsat time series. The extraction process is random and a final step is carried out to adjust the resulting rainy time replacing some events with others of the same peak attenuation class which fit better the requested rain time duration. To summarize, events are randomly picked from a database of events clustered by peak attenuation and duration to fit three conditions on: 1) the rainy time duration of each peak attenuation class as set by the objective CCDFs, 2) the distribution of the duration of the events as set by the underlying dry/rainy binary time series, and 3) the spatial-temporal features of the random processes involved. Note that, differently from the formulation in [19], where MTS events were broken into one-hour fixed periods and the binary dry/rainy periods had durations multiple of one-hour, here the original events in the databases are not manipulated to avoid harsh discontinuities in rain attenuation time series that would bias the simulation of FMTs.

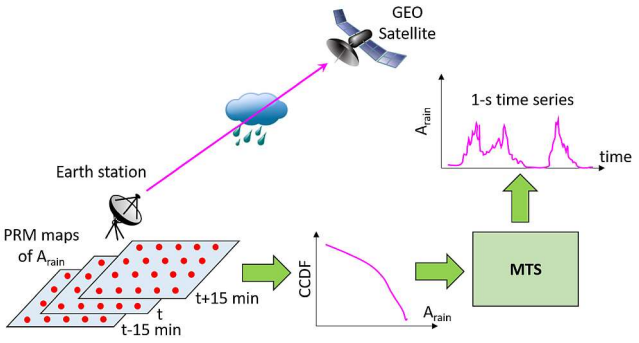

Fig. 3 Sketch of the stochastic interpolation methods executed by the MTS that generates 1-s time series of V-band rain attenuation from 15-min PRM time series. The simple case of one station is considered even though MTS can produce time series in several locations reproducing the spatial-correlation of the process.

The MTS time series of rain attenuation are linked to the PRM time series in a first order statistical sense, as they reproduce the objective CCDF relative to the observation period, but the correlation in the time domain is not preserved. The MTS has been designed and mainly used so far to reproduce the climatological CCDF of rain attenuation, generating long time series (e.g. one to several years). Here, the MTS is used to resample the 15-min resolution time series down to 1-sec resolution during shorter observation windows. In this case, the agreement between the resulting CCDF and the objective one will depend on two factors: 1) the shape of the objective CCDF, which can be irregular when derived from observation of rainfall occurrence over a relatively short time window, and 2) the capability of the MTS to reproduce the objective CCDF regardless of its shape, by combining only a few database events. These aspects will be further discussed in section III.C, where the MTS outcomes will be assessed against the objective CCDFs. Note that CCDFs are sensitive to the sampling time. If we build a CCDF from a population of N-samples of a stationary random process, we can state that the CCDF based on N samples will match the asymptotic CCDF (i.e. when $N=+inf$) down to a minimum exceedance probability level $P_{min}>1/N$. In our case, assuming $P_{min}=10/N$ and having 15-min data over 28 days from the PRM simulations, the corresponding CCDF will be reliable down to about $P_{min}=0.4\%$ that should be a reference level to keep in mind in performing comparison with other databases.

III. Model Chain Validation

Two different sets of measurements are used to validate the model chain:

- radiosonde data from 47 sites across Europe (red dots in Fig. 2) collected twice a day, at 00:00 and 12:00 UTC, respectively;
- measurements collected during the Alphasat experiment by the Italian receivers in Tito Scalo and Spino d'Adda (TS and SdA in Fig. 2, respectively) in terms of beacon attenuation at 19.7 GHz and 39.4 GHz at elevation angles of 42.1° and 35.5°, respectively.

The validation activity is carried out over a period of time covering 28 non-consecutive days in April-May 2020, selected in order to monitor different meteorological conditions and to maximize the availability of the Alphasat measurements at the two ground stations of Tito Scalo and Spino d'Adda. The number of days selected (28) is a compromise between satisfying the above conditions and keeping reasonable values of both computational times and size of the overall data produced by the NWP simulations.

A. NWP Model Validation

The NWP performance is analyzed by comparing the model output with rawinsonde data (RAwindsonde Observation program, RAOB) from 47 sites across Europe (Fig. 2) for the test week 25-31 May 2020. The Root Mean Squared (RMS) error for the vertical profiles of temperature, water vapor, and relative humidity is then calculated as follows. The RAOB profiles are interpolated on the model levels and compared to the model profiles from the model grid point closest to each available rawinsonde site. Fifty-one levels in the vertical are used. The vertical spacing is on the order of tens of meters for the levels nearest the ground and gradually increases with height. The model top is fixed at 40 hPa, which corresponds to a height of about 21/22 km above the ground level. The comparison is carried out at 00:00 and 12:00 UTC over the selected timeframe. For the comparison at 12:00 UTC, the 6-h NWP forecast from the run initialized at 06:00 UTC is used and, similarly, for the comparison at 00:00 UTC, the 6-h NWP forecast from the run initialized at 18:00 UTC is used.

Fig. 4, Fig. 5 and Fig. 6, show the statistics for temperature (T), water vapor mixing ratio (r) and relative humidity (RH) obtained by including the 94 daily radio-soundings (47 sites, 2 launches per day), over the considered seven days. The vertical profiles considered are 652 out of 47×2×7 = 658 because six radio-soundings were not available. The left panel of each figure shows the mean (μ) and the standard deviation (σ) of the NWP and RAOB vertical profiles (in blue and red, respectively):

- μ_T^{RAOB}, μ_T^{NWP}, σ_T^{RAOB}, σ_T^{NWP}: mean and standard deviation of T from RAOB and NWP vertical profiles;
- μ_r^{RAOB}, μ_r^{NWP}, σ_r^{RAOB}, σ_r^{NWP}: mean and standard deviation of r from RAOB and NWP vertical profiles;

- μ_{RH}^{RAOB}, μ_{RH}^{NWP}, σ_{RH}^{RAOB}, σ_{RH}^{NWP}: mean and standard deviation of *RH* from RAOB and NWP vertical profiles;

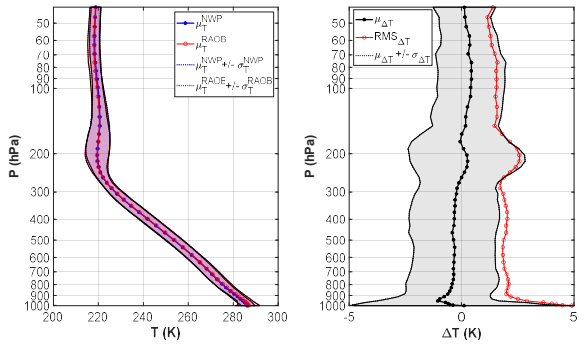

(a) (b)

Fig. 4 Validation of the temperature *T* as predicted from NWP on different vertical pressure levels *P*: (a) mean and standard deviation of vertical profile for radiosondes (red) and the NWP 6-hour model forecast (blue); (b) mean (black), standard deviation (gray) and RMS (red) of the differences between radiosondes and forecasts.

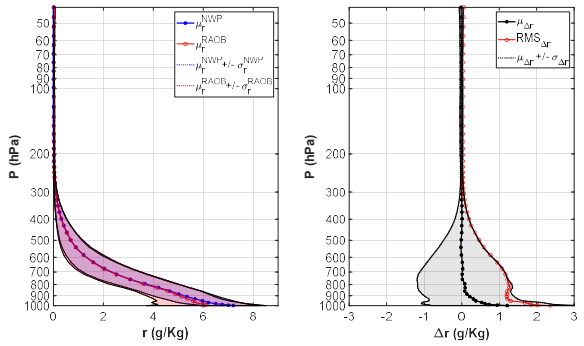

(a) (b)

Fig. 5 Validation of the water vapor mixing ratio *r* predicted by NWP on different vertical pressure levels *P*: (a) mean and standard deviation of vertical profile for radiosondes (red) and the NWP 6-hour model forecast (blue); (b) mean (black), standard deviation (gray) and RMS (red) of the differences between radiosondes and model forecasts.

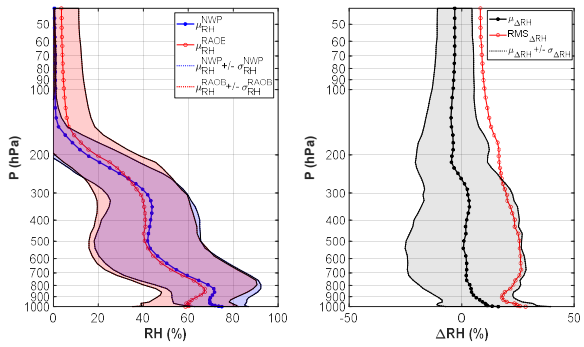

(a) (b)

Fig. 6 Validation of the relative humidity *RH* predicted by NWP on different vertical pressure levels *P*: (a): mean and standard deviation of vertical profile for radiosondes (red) and the NWP 6-hour model forecast (blue); (b) mean (black), standard deviation (gray) and RMS (red) of the differences between radiosondes and model forecasts.

The right panels show the mean (black), standard deviation (gray) and RMS (red) of the differences between the forecasts and the observations, denoted as $\mu_{\Delta x}$, $\sigma_{\Delta x}$ and $RMS_{\Delta x}$, where x represents the considered variable (*T*, *r* or *RH*), and $\Delta x = x^{NWP} - x^{RAOB}$. The NWP forecast exhibits a slight negative temperature bias in the lower troposphere of less than 1 K, between 400 and 1000 mb (Fig. 4), and a positive bias of about 1g/kg or less in water vapor mixing ratio in the same layer, decreasing with altitude (Fig. 5). The combination of these biases result in an overall positive relative humidity bias, higher and up to 35% in the lowest boundary layer and lower troposphere, then decreasing at higher altitudes (Fig. 6). Such errors are deemed acceptable and consistent with findings from previous works [38].

B. PRM Validation

PRM is run over the entire European domain at 15-min time resolution. Fig. 7 shows an example of the attenuation and the brightness temperature computed over the European domain at two different frequencies on the test day of 25/05/2020 at 20:00 UTC. Similar plots are available for all the simulated frequencies and the simulated four weeks.

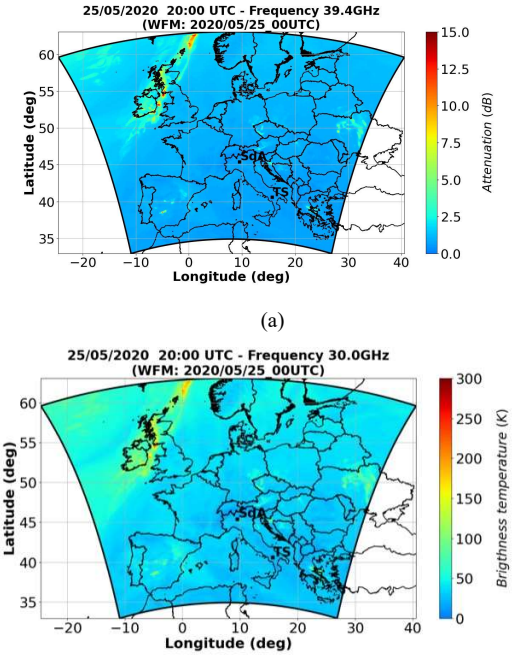

(a)

(b)

Fig. 7 Example of PRM output over the European domain (9 km×9 km grid) on 25/05/2020 at 20:00 UTC: (a) total attenuation at 39.4 GHz; (b) brightness temperature at 30.0 GHz.

The model validation is performed through a statistical comparison between PRM simulations and Alphasat beacon measurements at Tito Scalo and Spino d'Adda, based on the CCDF of path attenuation over the 28-days observation period. As for path attenuation, the two Alphasat frequencies are considered, i.e. 19.7 and 39.4 GHz. The results are shown in Fig. 8 where the blue curves are the CCDFs of the beacon data and the green and red curves are the CCDF relative to:

- "PRM (d01)": obtained by running PRM over the entire d01 European domain using as input the full NWP output database;
- "PRM (single grid-point)": obtained by running PRM

over the two grid-points corresponding to the Alphasat receiving stations of Tito Scalo and Spino d'Adda, using as input data the recorded NWP high-temporal resolution timeseries.

Before discussing the results, it is important to remark that:

- Alphasat processed measurements have been averaged over a 60-sec time window, from the original sampling rate of 16 sample/sec, in order to smooth the scintillation effects; PRM simulations over the station single grid-point are resampled from 30-sec to 60-sec (by averaging values over a 60-sec time-window) in order to have the same time step as Alphasat processed measurements; PRM simulations over the European domain have a much larger time step of 15-min;
- Alphasat measurements are at an elevation of 42.1° in Tito Scalo and 35.5° in Spino d'Adda, while PRM simulations are performed at zenith and scaled at the Alphasat elevation by using the cosecant law;
- Alphasat data are point measurements, even though averaged over the link path, while PRM simulations are obtained from a regional scale model which implies a spatial averaging process over the geographical area of interest with a single grid-point with 9 km × 9 km resolution;
- PRM CCDFs relative to the European domain, cyan line, are derived from the median values of the attenuation computed over a 3 × 3 points grid centered around the considered ground station. This helps to mitigate the well-known NWP models issue in correctly predicting a meteorological event both in space and in time, also known as double-penalty error [39].

Fig. 8 highlights a good agreement with Alphasat measurements in clear and cloudy atmosphere (i.e. down to about 5% of time) in both Tito Scalo and Spino d'Adda and with both PRM (d01) and PRM (single grid-point) simulations. The results are different in rainy conditions:

- in Tito Scalo: while the PRM (single grid-point) overestimates the attenuation, the PRM (d01) is in good agreement with measurements;
- in Spino d'Adda: the two PRM simulations exhibit a similar trend and overestimate the attenuation.

The different behavior of the two PRM simulations observed in Tito Scalo with respect to Spino d'Adda are probably due to the orographic differences. Indeed, the area surrounding Tito Scalo is characterized by mountainous reliefs while the terrain around Spino d'Adda is flat. The orography may affect the precipitation and its distribution over the area of interest. Specifically, in Tito Scalo we expect rain events focused in small geographical areas that, in turns, are difficult to be predicted through NWP models thus causing strong overestimations of the precipitation. In this sense, the spatial median value calculated over the 3×3 points grid helps to mitigate such overestimation in Tito Scalo (where a huge scatter among the nearby grid-points is observed due to the complex orography) while, as expected, the same average has no effect in Spino d'Adda.

The errors between PRM-simulated and Alphasat-measured CCDFs are quantified in Table II and Table III for Tito Scalo and Spino d'Adda, respectively, in terms of mean B (dB) and standard deviation σ_B (dB) of the absolute error $(\tilde{x}_i - x_i)$ where x and $\tilde{x}$ are the measured and simulated values of attenuation at fixed percentage of time, respectively. Nine equally-spaced points per decade have been considered ranging from 0.1% to 100%.

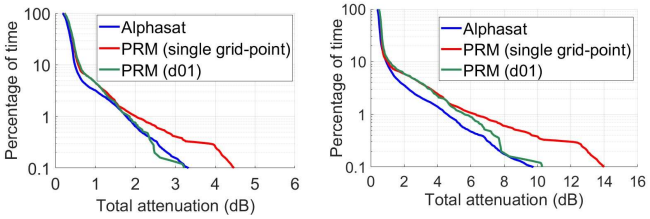

(a) Tito Scalo, 19.7 GHz (b) Tito Scalo, 39.4 GHz

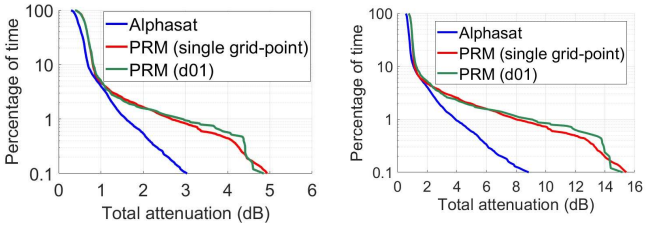

(c) Spino d'Adda, 19.7 GHz (d) Spino d'Adda, 39.4 GHz

Fig. 8 PRM validation vs Alphasat measurements in terms of exceedance probability of attenuation calculated over the 4 simulated weeks: Tito Scalo (top panels) and Spino d'Adda (bottom panels) at 19.4 GHz (left panels) and 39.4 GHz (right panels).

TABLE II
ERRORS BETWEEN PRM-SIMULATED AND ALPHASAT-MEASURED CCDFS OF TOTAL ATTENUATION OVER 4 WEEKS IN TITO SCALO

	PRM		PRM single grid-point	
Frequency	**19.7 GHz**	**39.4 GHz**	**19.7 GHz**	**39.4 GHz**
***B* (dB)**	0.07	0.59	0.32	1.36
σ_B (dB)	0.11	0.47	0.35	1.51

TABLE III
ERRORS BETWEEN PRM-SIMULATED AND ALPHASAT-MEASURED CCDFS OF TOTAL ATTENUATION OVER 4 WEEKS IN SPINO D'ADDA

	PRM		PRM single grid-point	
Frequency	**19.7 GHz**	**39.4 GHz**	**19.7 GHz**	**39.4 GHz**
***B* (dB)**	0.74	2.65	0.66	2.31
σ_B (dB)	0.83	3.17	0.72	2.77

C. *Multisite Time series Synthesizer Validation*

MTS simulations were carried out over the 28-days observation period, synthesizing time series of rain attenuation at 39.4 GHz in Tito Scalo and Spino d'Adda, starting from three different objective CCDFs:

- Alphasat beacon measurements;
- PRM (d01) forecasts;
- PRM (single grid-point) forecasts.

Following the approach illustrated in the previous section, the 15-min PRM forecast data are taken as the median value calculated from the 3×3 grid-points centered about the considered station (Tito Scalo or Spino d'Adda), while 30-sec data are generated by PRM at the grid-point including the specific site location. The validation process is carried out by

comparing the CCDFs obtained from the MTS time series with the objective CCDFs.

Fig. 9 shows the results. In each panel, the purple line is the objective CCDF, the black line is the CCDF obtained from the 28-days MTS time series, and, finally, the cyan line is the CCDF that can be asymptotically achieved by MTS, when all the events in the database are combined together. Specifically, the CCDF in cyan is obtained by dividing the events in the dataset in classes, according to their peak attenuation, building the CCDF of each class and fitting a linear combination of these CCDFs to the objective CCDF. Hence, the difference between the black and the cyan curves is due to the limited capability of MTS to reproduce an objective CCDF, when a relatively short period of time is considered, i.e. when only few events are extracted from the database, as is the case of the 28-day test window. On the other hand, the difference between the purple and the cyan curves increases when the objective CCDF has an irregular shape, i.e., it is difficult to reproduce. Despite the objective CCDFs of rain attenuation returned by PRM are rather lumpy, the black curves provide a good agreement at least down to 0.1% of time, i.e. about 40 minutes. The black and cyan lines are close together, which means that the error due to short duration of the time series is small. The distance between black and purples curves increases when the patterns of the objective CCDFs are bumpy, as in the case of PRM data at Tito Scalo. The errors between MTS-simulated and objective CCDFs are quantified in Table IV and Table V for Tito Scalo and Spino d'Adda, respectively, with the same criterion of Table II and Table III.

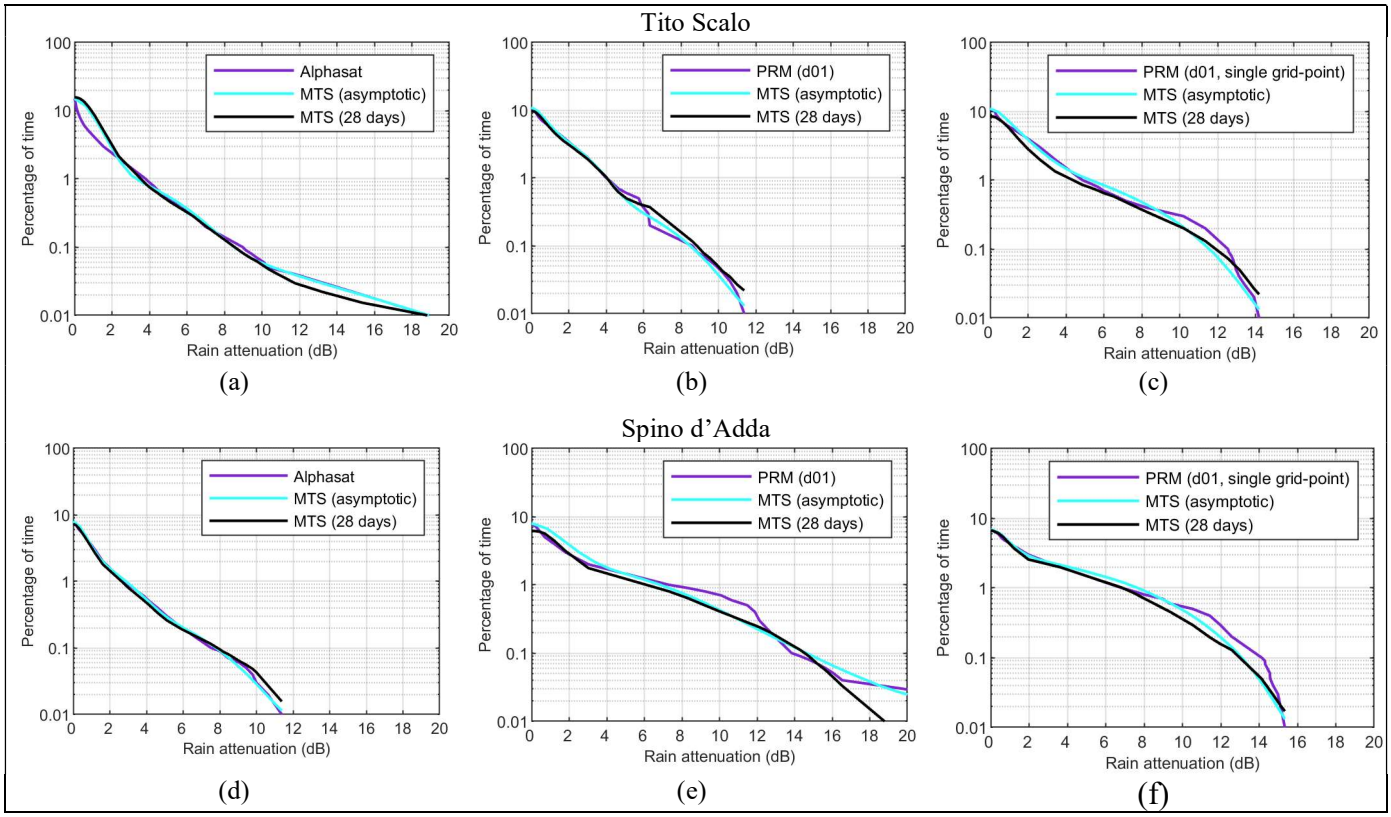

Fig. 9 MTS validation: CCDFs of Q-band rain attenuation generated by MTS over a 28-day period against the objective CCDFs at Tito Scalo (top) and Spino d'Adda (bottom). The objective CCDFs are: Alphasat beacon measurements at 60-sec (left), PRM d01 forecasts at 15-min generated over the European domain and averaged over the 3 × 3 grid-points centered about the ground-station (middle), PRM d01 single grid-point forecasts at 60-sec generated in the two sites (right).

TABLE IV
ERRORS BETWEEN MTS-SIMULATED AND OBJECTIVE CCDFS OF RAIN ATTENUATION: OVER 4 WEEKS IN TITO SCALO

Objective	Alphasat	PRM	PRM single grid-point
B **(dB)**	0.21	0.04	-0.50
σ_B **(dB)**	0.49	0.43	0.37

TABLE V
ERRORS BETWEEN MTS-SIMULATED AND OBJECTIVE CCDFS OF RAIN ATTENUATION OVER 4 WEEKS IN SPINO D'ADDA

Objective	Alphasat	PRM	PRM single grid-point
B **(dB)**	-0.13	-0.87	-0.64
σ_B **(dB)**	0.17	1.00	0.61

The results in Fig. 9, Table IV and Table V indicate that the MTS can fit very different CCDF shapes. However, the temporal synchronization between the 1-sec time series and the input 15-min PRM time axis is lost. Hence, to synthesize 1-sec time series of total attenuation adding up rain attenuation produced by the MTS to gas and cloud attenuation, the last two must are re-generated as described in the following.

For the gas attenuation, we have adopted the link budget engineer's perspective, setting up a constant value corresponding to the 99th percentile of the CCDF of gas attenuation simulated by PRM in each site, that is, a conservative estimate for gas attenuation.

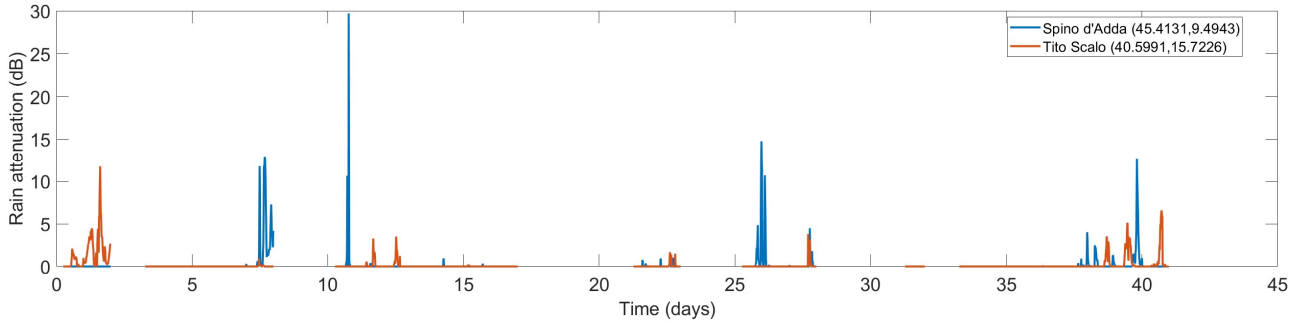

(a)

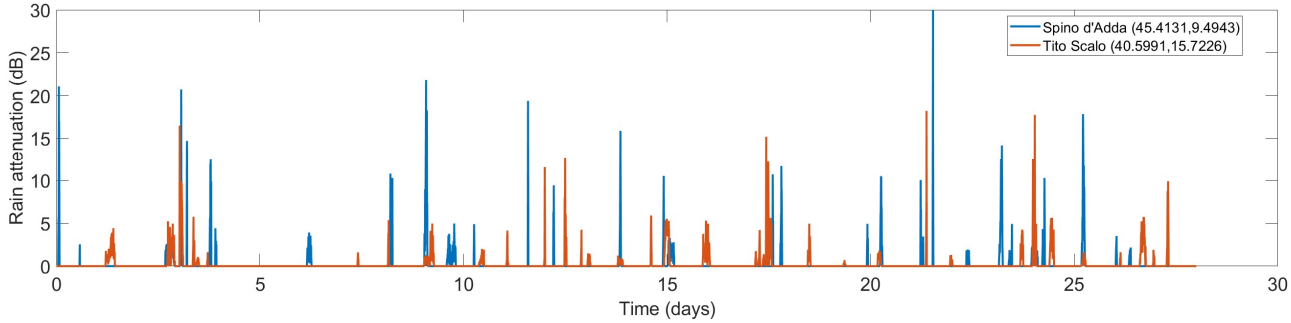

(b)

Fig. 10 Time series generation of rain attenuation: (a) simulated by PRM(d01) with 15-min time step (empty spaces in the time-axis are due to the fact that the 28 simulated days are not consecutive); (b) generated by MTS with 1-sec time step (28 consecutive days are generated).

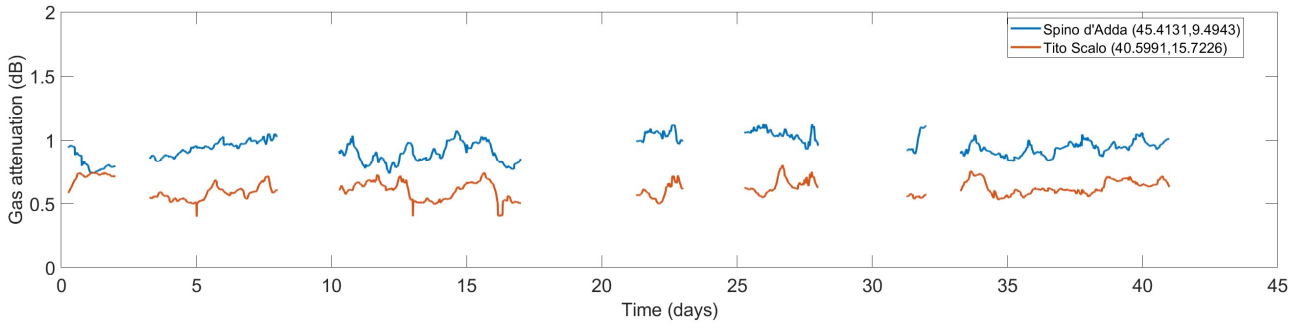

(a)

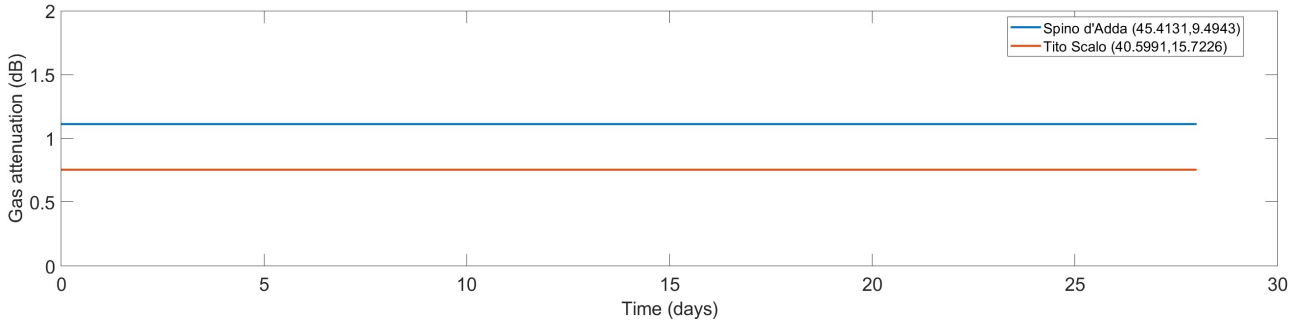

(b)

Fig. 11 Time series generation of gas attenuation: (a) simulated by PRM(d01) with 15-min time step (empty spaces in the time-axis are due to the fact that the 28 simulated days are not consecutive); (b) generated by MTS with 1-sec time step (28 consecutive days are generated).

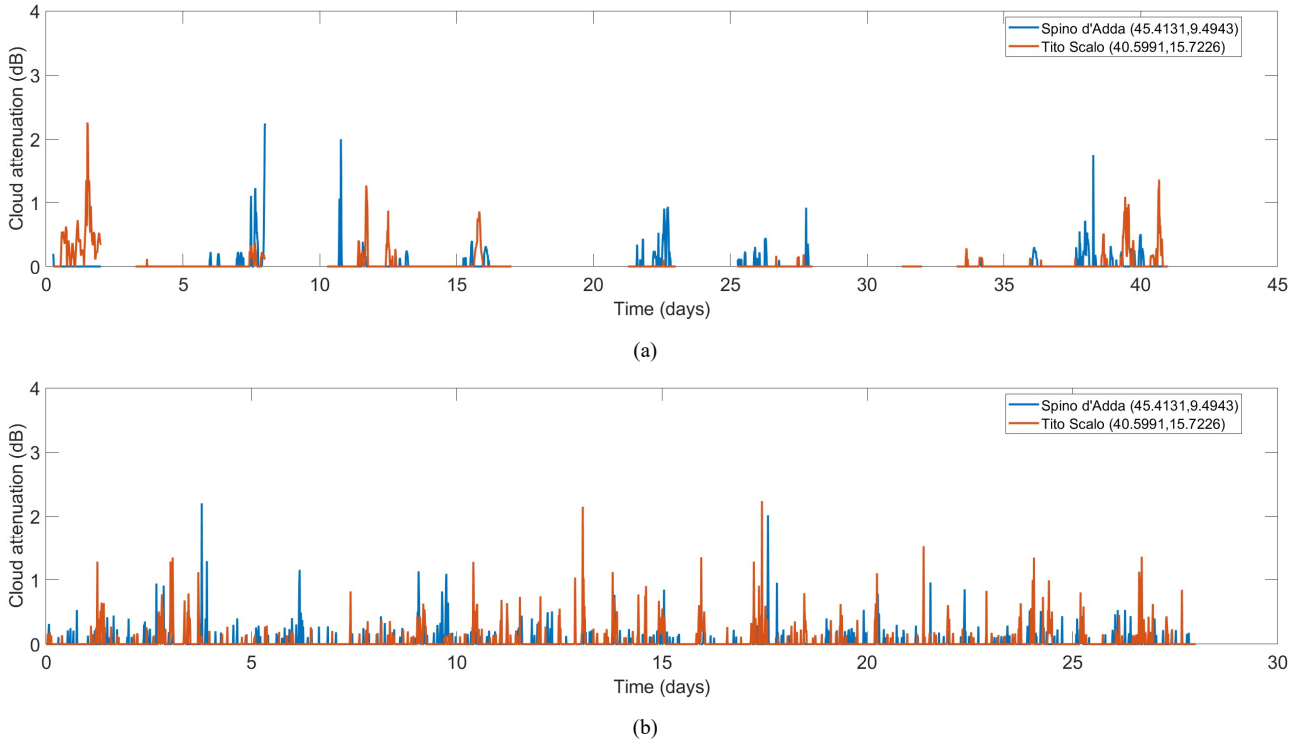

Fig. 12 Time series generation of cloud attenuation: (a) simulated by PRM(d01) with 15-min time step (empty spaces in the time-axis are due to the fact that the 28 simulated days are not consecutive); (b) generated by MTS with 1-sec time step (28 consecutive days are generated).

Cloud attenuation time series in each site are obtained through the following procedure:

- separate dry and wet time instants in the PRM time series;
- calculate the CCDF of cloud attenuation A_{cl} in the dry and wet PRM intervals, namely $P(A_{cl} \mid \text{dry})$ and $P(A_{cl} \mid \text{wet})$;
- consider the 1-sec time series of MTS rain attenuation:
  - pick a random value of cloud attenuation every 15-min from $P(A_{cl} \mid \text{dry})$ or $P(A_{cl} \mid \text{wet})$ depending on whether the corresponding MTS sample of rain attenuation is dry or wet;
  - linearly interpolate the series over the 1-sec MTS time axis.

Fig. 10, Fig. 11 and Fig. 12 show the attenuation time series generated by MTS starting from the corresponding PRM time series for the rain, gas and cloud component, respectively, at Tito Scalo and Spino d'Adda. Note that, panels (a) of the figures show time-series simulated with PRM over the selected 28 non-consecutive days, that explains the empty spaces in the time-axis, while panels (b) show the time series generated by MTS. The latter always covers a period of 28 days but, in this case, they are consecutively generated.

IV. Conclusions and Future Work

The objective of this work was to demonstrate the potential of an NWP-based tool for the design of a SatCom system that implements FMTs to carry out the channel assessment for the satellite link. Starting from the physical background provided by an NWP model, we propose a methodology to generate time series of the path attenuation for SatCom applications, specifically to simulate the operation of adaptive FMTs at Ka-band and beyond, suffering from severe propagation impairments. To this aim, a parametric, physically-based radiopropagation model (PRM) is cascaded with the outputs of the NWP model. It converts the 3D fields of the NWP meteorological outputs into 3D fields of the specific attenuation due to gas, clouds and rain. The attenuation over each earth-to-satellite path is then obtained through the simple cosecant rule from the attenuation calculated along the zenith.

The data are generated over a 400 × 350 points grid covering Europe with a resolution of 9 km × 9 km in space and 15-min in time, respectively. As NWP runs are time consuming and data-intensive, these settings are a trade-off between providing propagation data over the large SatCom coverage areas and achieving a resolution in time and space fine enough to track channel variations, mostly due to rain. To handle the rapidly changing rain attenuation, the resolution in time has been further increased to 1-sec by adding a third block (MTS) to the chain. MTS generates time series of dry/rainy periods in multiple sites and fills every rainy slot with rain events extracted from a dataset of beacon attenuation measurements during Italsat experiment. The extraction process is stochastic but bounded to reproduce the CCDF of the PRM-based rain attenuation.

Each of the three blocks of the model-chain was validated through comparison with ground-based measurements. NWP outputs are validated against radio-sounding observations in 47 sites all over Europe, in terms of vertical profiles of temperature, water vapor mixing ratio and relative humidity, highlighting a very good agreement between measurements and predictions also in line with previous studies. The CCDFs

produced by PRM and MTS were validated exploiting measurements available from the two Italian Alphasat beacon receivers (in Tito Scalo and Spino d'Adda) in terms of attenuation at 19.7 GHz (Ka-band) and 39.4 GHz (Q-band) over a 28-day period. The validation shows a very good agreement between PRM-simulations and Alphasat measurements in clear and cloudy sky conditions. In rainy conditions, PRM tends to overestimate attenuation up to a maximum of about 2 dB at 19.7 GHz and 7 dB at 39.4 GHz. The effects of a complex orography (such the one in Tito Scalo) on the NWP+PRM cascade, combined with the space-time averaging process, result into a mitigation of such overestimation. The MTS fits fairly well the first-order statistics of rain attenuation over the relatively short validation period, down to percentages of time corresponding to less than one hour per year, providing an effective way to resample time series with a coarse time step into 1–sec time series. Gas attenuation and cloud attenuation, which are less critical for FMT assessment, are resampled with simpler methods.

Although the temporal correlation between PRM and MTS rainy events is lost, the MTS ability in correctly reproducing the objective statistics confirms the reliability of the proposed model-chain and its potentiality in future application of SatCom systems for the implementation of FMTs. Future works will be devoted to refining the current radiopropagation model as well as to test different procedures for the rainy event extraction process of the MTS. Alternative solutions to the cosecant law will be investigated, for example physically-based radiopropagation models that are able to resolve the radiative transfer equation along the slant-path, such the ones adopted in [38], [39]. This approach is expected to mitigate the PRM overestimation trend. Finally, the whole model-chain will be tested for FMTs implementation within a SatCom system framework.

ACKNOWLEDGEMENTS

Acknowledgements goes to: the European Space Agency (ESA) for partially supporting this activity under the ESA-ESTEC contract No. 4000133554/21/NL/AF "RadioSatMet: Short-term forecast of RADIOcommunication geostationary SATellite links coupling METeorological space-time models, radiative transfer algorithms and ground-terminal data" ARTES AT 3B.037; AdaptiveMeteo for the validation work of WRF against rawinsondes observations carried out within the RadioSatMet project; HIMET for the computing and storage resources provided for the large amount of data produced by both the NWP and the PRM models runs carried out within the RadioSatMet project; Livio Bernardini (HIMET) for his contribution in running the NWP model and interpreting the results within the RadioSatMet project; the Agenzia Spaziale Italiana (ASI), in particular Giuseppe Codispoti and Giorgia Parca, for supporting the Alphasat Aldo Paraboni propagation experiment.

REFERENCES

[1] P. Thompson, B. Evans, L. Castenet, M. Bousquet, and T. Mathiopoulos, "Concepts and Technologies for a Terabit/s Satellite", The Third International Conference on Advances in Satellite and Space Communications (SPACOMM 2011), April 17-22, 2011 Budapest, Hungary.

[2] G. Brussaard, and P.A .Watson, "Atmospheric modelling and millimetre wave propagation". London : Chapman & Hall, 1995. 329 p.

[3] C. Capsoni, (editor), "Verification of propagation impairment mitigation techniques. Final Report of the ESA/ESTEC Contract No. 20887/07/NL/LvH, 2011.

[4] ArianeGroup, "Ariane 5 successfully launches the innovative EUTELSAT KONNECT VHTS satellite", https://www.arianespace.com/press-release/ariane-5-successfully-launches-the-innovative-eutelsat-konnect-vhts-satellite/

[5] Rachel Jewett, Via Satellite, "SpaceX Launches Long-Awaited Hughes Jupiter 3 Satellite", https://www.satellitetoday.com/launch/2023/07/30/spacex-launches-long-awaited-hughes-jupiter-3-satellite/

[6] L. Luini, "A Comprehensive Methodology to Assess Tropospheric Fade Affecting Earth–Space Communication Systems," in IEEE Transactions on Antennas and Propagation, vol. 65, no. 7, pp. 3654-3663, July 2017, doi: 10.1109/TAP.2017.2700883.

[7] T. Rossi, M. De Sanctis and F. Maggio, "Evaluation of Outage Probability for Satellite Systems Exploiting Smart Gateway Configurations," in IEEE Communications Letters, vol. 21, no. 7, pp. 1541-1544, July 2017, doi: 10.1109/LCOMM.2017.2684810.

[8] A. Paraboni et al., "Meteorology-Driven Optimum Control of a Multibeam Antenna in Satellite Telecommunications," in IEEE Transactions on Antennas and Propagation, vol. 57, no. 2, pp. 508-519, Feb. 2009, doi: 10.1109/TAP.2008.2011238.

[9] S. Ventouras and P. -D. Arapoglou, "Assessment of Practical Smart Gateway Diversity Based on Multisite Measurements in Q-/V-Band," in IEEE Transactions on Antennas and Propagation, vol. 69, no. 6, pp. 3427-3435, June 2021, doi: 10.1109/TAP.2020.3044370.

[10] J. P. V. P. Baptista et al., "OPEX: Second Workshop of the OLYMPUS propagation experimenters. Volume 1: Reference book on attenuation measurement and prediction," p. 8, Nov. 1994.

[11] F. Fedi, A. Paraboni, A. Martinelli, and A. Vincenti, "The Italsat program: The propagation experiment," Rivista Tecnica Selenia. Italsat Special Issue, vol. III, no. 4, pp. 40–59, 1990.

[12] B. R. Arbesser-Rastburg and A. Paraboni, "European research on Ka-band slant path propagation," in Proceedings of the IEEE, vol. 85, no. 6, pp. 843-852, June 1997, doi: 10.1109/5.598408.

[13] C. Riva, A. Martellucci (Guest editors), International Journal of Satellite Communications and Networking, Special Issue: Alphasat Aldo Paraboni Ka and Q/V experiment, vol. 37, no. 5, September/October 2019, pp. 385-386 (DOI: 10.1002/sat.1314, Print ISSN: 1542-0973, Online ISSN: 1542-0981)

[14] R. De Gaudenzi, E. Re and P.Angeletti. "Smart Gateways Concepts for High-Capacity Multi-beam Networks," AIAA 2012-15238. 30th AIAA International Communications Satellite System Conference (ICSSC). September 2012.

[15] R. Kumar and S. Arnon, "Experimental Modeling of Short-Term Effects of Rain on Satellite Link Using Machine Learning," in IEEE Transactions on Instrumentation and Measurement, vol. 72, pp. 1-12, 2023, Art no. 5503812, doi: 10.1109/TIM.2023.3306825.

[16] International Telecommunication Union (ITU), Time series synthesis of tropospheric impairments, Recomm. P. 1853–2, Geneva, Switzerland, 2019.

[17] T. Maseng and P. Bakken, "A Stochastic Dynamic Model of Rain Attenuation," in IEEE Transactions on Communications, vol. 29, no. 5, pp. 660-669, May 1981, doi: 10.1109/TCOM.1981.1095044.

[18] G. Carrie, Lacoste, F. and Castanet, L. (2011), A new 'event-on-demand' synthesizer of rain attenuation time series at Ku-, Ka- and Q/V-bands. Int. J. Satell. Commun. Network., 29: 47-60. https://doi.org/10.1002/sat.951

[19] R. Nebuloni, Capsoni, C., and Luccini, M. (2014), Advanced time series synthesizer for simulation of joint rain attenuation conditions, Radio Sci., 49, 699– 708, doi:10.1002/2014RS005541.

[20] M. Biscarini et al., "Weather effects mitigation at Ka band by using radiometeorological model forecast in deep space downlinks," 2015 9th European Conference on Antennas and Propagation (EuCAP), Lisbon, Portugal, 2015, pp. 1-5.

[21] M. Outeiral García, N. Jeannin, L. Féral and L. Castanet, "Use of WRF model to characterize propagation effects in the troposphere," 2013 7th European Conference on Antennas and Propagation (EuCAP), Gothenburg, Sweden, 2013, pp. 1377-1381.

[22] N. Jeannin et al., "Atmospheric channel simulator for the simulation of propagation impairments for Ka band data downlink," The 8th European Conference on Antennas and Propagation (EuCAP 2014), The Hague, Netherlands, 2014, pp. 3357-3361, doi: 10.1109/EuCAP.2014.6902547.

[23] N. Jeannin, Castanet, L, Dahman, I, Pourret, V, Pouponneau, B. Smart gateways switching control algorithms based on tropospheric propagation forecasts. Int J Satell Commun Network. 2019; 37: 43– 55. https://doi.org/10.1002/sat.1233.

[24] M. Razavian, Oestges, C., & Vanhoenacker-Janvier, D. (2023). Synthetic rain models and optical flow algorithms for improving the resolution of rain attenuation time series simulated from Numerical Weather Prediction. Radio Science, 58, e2022RS007553. https://doi.org/10.1029/2022RS007553

[25] M. Biscarini et al., "Short-term Forecast of Radiocommunication Geostationary Satellite Links coupling Weather Prediction and Radiopropagation Models," 2022 16th European Conference on Antennas and Propagation (EuCAP), Madrid, Spain, 2022, pp. 1-5, doi: 10.23919/EuCAP53622.2022.9769013.

[26] R. Nebuloni et al., "Exploiting Numerical Weather Prediction Data for Radiopropagation Modeling of SatCom Links," 2024 18th European Conference on Antennas and Propagation (EuCAP), Glasgow, United Kingdom, 2024, pp. 1-5, doi: 10.23919/EuCAP60739.2024.10501034.

[27] Skamarock, W. C., J. B. Klemp, J. Dudhia, D. O. Gill, Z. Liu, J. Berner, W. Wang, J. G. Powers, M. G. Duda, D. M. Barker, and X.-Y. Huang, 2019: A Description of the Advanced Research WRF Version 4. *NCAR Tech. Note NCAR/TN-556+STR*, 145 pp. doi:10.5065/1dfh-6p97 .

[28] L. Luini and C. Capsoni, "Scaling Cloud Attenuation Statistics With Link Elevation in Earth-Space Applications," in IEEE Transactions on Antennas and Propagation, vol. 64, no. 3, pp. 1089-1095, March 2016, doi: 10.1109/TAP.2016.2521872.

[29] L. M. Tomaz, C. Capsoni and L. Luini, "Scaling Rain Attenuation as a Function of the Link Elevation," 2018 2nd URSI Atlantic Radio Science Meeting (AT-RASC), Gran Canaria, Spain, 2018, pp. 1-4, doi: 10.23919/URSI-AT-RASC.2018.8471390.

[30] C. Riva, L. Luini, R. Nebuloni, A. Marziani, F. Consalvi, F. S. Marzano, "The Alphasat Aldo Paraboni Propagation Experiment: Measurement Campaign at the Italian Ground Stations", International Journal of Satellite Communications and Networking, Vol. 37, Issue 5, Special Issue: Alphasat Aldo Paraboni Ka and Q/V experiment, pp. 423-436, September/October 2019.

[31] Ulaby, F., Moore. (1981). Microwave remote sensing: Active and passive, volume 3 [Book]. Artech House

[32] Mishchenko, M. I., Travis, L. D., & Lacis, A. A. (2006). Multiple scattering of light by particles: Radiative transfer and coherent backscattering. Cambridge: Cambridge University Press.

[33] Mishchenko, Michael I. et al. "T-matrix theory of electromagnetic scattering by particles and its applications: a comprehensive reference database." Journal of Quantitative Spectroscopy & Radiative Transfer 88 (2004): 357-406.

[34] M. Biscarini and F. S. Marzano, "Generalized Parametric Prediction Model of the Mean Radiative Temperature for Microwave Slant Paths in All-Weather Condition," in IEEE Transactions on Antennas and Propagation, vol. 68, no. 2, pp. 1031-1043, Feb. 2020, doi: 10.1109/TAP.2019.2943415.

[35] C. Riva, "Seasonal and diurnal variations of total attenuation measured with the ITALSAT satellite at Spino d'Adda at 18.7, 39.6 and 49.5 GHz," Int. J. Satellite Commun., vol. 22, pp. 449–476, 2004.

[36] A. Paraboni, and F. Barbaliscia, Multiple site attenuation prediction models based on the rainfall structures (meso- or synoptic-scales) for advanced TLC or broadcasting systems, 27th General Assembly of the International Union of Radio Science, URSI, Maastricht, Netherlands, 2002.

[37] International Telecommunication Union (ITU), Propagation data and prediction methods required for the design of Earth-space, telecommunication systems, Recomm. P. 618–13, Geneva, Switzerland, 2017.

[38] M. Biscarini, K. De Sanctis, S. Di Fabio, M. Montopoli, L. Milani and F. S. Marzano, "Assessment and Uncertainty Estimation of Weather-Forecast Driven Data Transfer for Space Exploration at Ka- and X-Band," in IEEE Transactions on Antennas and Propagation, vol. 67, no. 5, pp. 3308-3322, May 2019, doi: 10.1109/TAP.2019.2899041.

[39] M. Biscarini et al., "Dynamical Link Budget in Satellite Communications at Ka-Band: Testing Radiometeorological Forecasts With Hayabusa2 Deep-Space Mission Support Data," in IEEE Transactions on Wireless Communications, vol. 21, no. 6, pp. 3935-3950, June 2022, doi: 10.1109/TWC.2021.3125751.

Marianna Biscarini (Senior Member, IEEE) received the M.Sc. degree (cum laude) in electronic engineering and the Ph.D. degree in electromagnetism from the Sapienza University of Rome, Italy, in 2012 and 2016, respectively. Since 2012, she has been with the Department of Information Engineering, Electronics and Telecommunications (DIET) of Sapienza University of Rome, and with the Center of Excellence in Telesensing of Environment and Model Prediction of Severe Events (CETEMPS) of University of L'Aquila, working on electromagnetic wave propagation through the atmosphere (especially at microwave frequencies): physical modeling for electromagnetic propagation applications, such as attenuation due to rain/ice particles, scintillation effects, and expected impact on satellilte links, remote sensing of atmospheric constituents using radiometric data, dimensioning of SatCom systems also exploiting weather forecast models and Propagation Impairment Mitigation Techniques (PIMT). She is currently a Research Assistant with DIET teaching the master's degree course on "Radiopropagation and radarmeteorology" and is involved in several international projects, most of them commissioned to the research group by the European Space Agency (ESA), the USA Air Force Laboratory (AFRL), and Thales Alenia Space Italy. She is Associate Editor of IEEE Geoscience and Remote Sensing Letters (GRSL) and member of the Italian Society of Electromagnetism.

Roberto Nebuloni received the Laurea degree in electronic engineering and the PhD degree in information engineering from the Politecnico di Milano, Milan, Italy in 1997 and 2004, respectively. In 1997-2005, he worked as a research associate at Politecnico di Milano. At the end of 2005, he joined the Italian National Research Council (CNR), where he is currently a researcher at the Institute of Electronics, Computer and Telecommunication Engineering (IEIIT), in Milan. His core research is on the modeling of mmWave and optical wave propagation through the atmosphere, adaptive SatCom systems and rain fade mitigation techniques. He participated in the European framework for Cooperation in Science and Technology (COST actions IC0802 and IC1101 focused on optical wireless communications) and in the Satellite Communications Network of Excellence (SatNEx). He has been involved in several projects funded by the European Space Agency (ESA) and focused on the study, design and implementation of propagation impairments mitigation techniques for advanced satellite systems. Recently he has been involved in the H2020 project named QV-LIFT (Q/V Band Earth Segment Link for Future High Throughput Space Systems) aimed at assessing the operation of Q-V band (i.e. 40-50 GHz) technology for the next-generation of telecommunication satellites. Finally, he is the principal investigator of the MOPRAM project (Monitoring of Precipitation through a Network of Microwave Radio Links), funded by Fondazione CARIPLO. Dr. Nebuloni is author of

about 70 papers published in international journals or international conference proceedings.

Laura Dossi graduated with honors in Electronic Engineering at Politecnico di Milano in 1985 and has been working since June 1988 as a researcher with CNR, from 2002 at Institute of Electronics, Computer and Telecommunication Engineering (IEIIT). Her core activities concern development and research in Information and Communications Technologies (ICT) area, with particular interest in satellite and wireless communications. She was involved in international experiments (Olympus satellite) and cooperated with other research centres (CSELT), universities (Politecnico di Milano) and telecommunication industries (Eutelsat, Italtel S.p.A., SIAE Microelettronica S.p.A., Siemens Mobile Communications S.p.A.). Recently she participated to the project THE4BEES (Transnational Holistic Ecosystem 4 Better Energy Efficiency through Social innovation), co-financed by the Alpine Space programme and collaborated with other CNR Institutes in a project commissioned by FINCANTIERI to design a prototype of a smart cabin ("E-Cabin")

Saverio Di Fabio received the Laurea degree in electrical engineering from the University of L'Aquila, L'Aquila, Italy. In 1997, he joined the Science and Technology Park of Abruzzo, L'Aquila, as a Microwave Engineer. From 2009 to 2012, he was a Radar Engineer with HIMET s.r.l., L'Aquila. Since 2012, he has been a Senior Scientist with CETEMPS, University of L'Aquila, where he has been working on radar systems and polarimetric data processing.

Paolo Scaccia earned the Master's degree in Theoretical Physics from the Sapienza University of Rome in September 2020 with a thesis on a comparative analysis of two different Hopfield models (neural network models). During the years of academic formation he collaborated to different research activities on satellite meteorology: in 2011 he supported the development and maintenance of the software UWPHYSRET (University of Wisconsin PHYsical RETrieval); from April 2014 to December 2015 he performed a Complexity Analysis for a prototype of a level 2 processor for MTG-IRS data (EUMETSAT); in 2016 he applied a Scale Analysis to the WRF forecast before and after the assimilation of the Transformed Retrievals produced by EUMETSAT. In july 2017 he co-founded with Dr. Antonelli Adaptive Meteo S.r.l. In the last two years he has been collaborating with the University of Hawaii in a study on the role of the Arctic Cyclogenesis in ice formation, and in the development of a python based inversion package for hyperspectral infrared space-borne data

Tiziana Cherubini received her M.Sc. degree (cum laude) in Physics from "La Sapienza" (Rome) and a PhD in Geophysics /Meteorology, from the University of Genoa (2001). She worked as graduate trainee in the Operations Department of the ECMWF focusing on the statistical validation of precipitation forecasts using non-conventional observations. As a post-doctoral fellow for the University of Hawaii in Manoa she worked on assimilating LIDAR wind data into the MM5 model. In 2003 she was hired as Research Meteorologist and Lead Modeler for the then recently founded Maunakea Weather Center. She is currently active in this position, while is also appointed affiliate Associate Researcher for the University of Hawaii, Manoa. Dr. Cherubini is primarily engaged in advancing meteorological forecasts for astronomical operations on Maunakea, Hawaii. She oversees and maintains a customized version of the WRF modeling system, handling operational responsibilities, and providing forecasts during the lead forecaster's absence. In addition, she focuses on developing optical turbulence prediction algorithms both within the context of the WRF model and using machine and deep learning techniques. She co-edited with Prof S. Businger the book Seeing Clearly - The impact of Atmospheric Turbulence on the Propagation of Extraterrestrial Radiation (2011) and supervised various doctoral and post-doctoral fellows and their projects. In recent years she collaborated with Adaptive Meteo s.r.l on EUMETSAT funded projects (MTG-IRS development), aimed to assimilate level 2 products derived from high spectral resolution data within the WRF forecast system. She is also currently contributing to the Office of Naval Research funded project "Advanced Use of Soundings from Hyperspectral IR Space-borne Observations to Improve Arctic Prediction".

Carlo Riva (Senior Member, IEEE) received the Laurea Degree in Electronic Engineering and the PhD degree in Electronic and Communication Engineering, from Politecnico di Milano, Milano, Italy, in 1990 and 1995, respectively. In 1999, he joined the Dipartimento di Elettronica, Informazione e Bioingegneria, Politecnico di Milano, where, since 2020, he has been a Full Professor of electromagnetic fields. He participated in the Olympus, Italsat and (the running) Alphasat Aldo Paraboni (for this experiment he has been appointed Principal Investigator by ASI in 2012) propagation measurement campaigns, in the COST255, COST280 and COSTIC0802 international projects on propagation and telecommunications and in the Satellite Communications Network of Excellence (SatNEx). He served as Associate Editor of IEEE Transactions on Antennas and Propagation in the period 2017-2023 and he is Chairman of WP 3J of ITU-R SG3 ('Propagation fundamentals'). He is the author of about 280 papers published in international journals or international conference proceedings. His main research activities are in the field of the tropospheric effects in satellite microwave links (GEO, MEO, LEO, Deep Space) and their statistical and physical modelling, the propagation impairment mitigation techniques and satellite communication adaptive systems.

Lorenzo Luini (Senior Member, IEEE) received the Laurea Degree (cum laude) in Telecommunication Engineering in 2004 and the Ph.D. degree in Information Technology in 2009 (cum laude) both from Politecnico di Milano, Italy. He is currently an Associate Professor at DEIB (Dipartimento di Elettronica, Informazione e Bioingegneria) of Politecnico di Milano. His research activities are focused on electromagnetic wave propagation through the atmosphere, both at radio and optical frequencies. He has been involved in several European COST projects, in the European Satellite Network of Excellence (SatNEx), as well as in several projects commissioned to the research group by the European Space Agency (ESA), the USA Air Force Laboratory (AFRL) and the European Commission (H2020). Lorenzo Luini authored 240 contributions to

international conferences and scientific journals. He is Associate Editor of IEEE Transactions on Antennas and Propagation (TAP) and of International Journal on Antennas and Propagation (IJAP), member of the Italian Society of Electromagnetism, Chair of the Working Group “Propagation” of EurAAP (European Association on Antennas and Propagation) and Leader of Working Group “Propagation data calibration” within the AlphaSat Aldo Paraboni propagation Experimenters (ASAPE) group.